Rapid Aqueous-Phase Oxidation of An *α*-Pinene-Derived Organosulfate by Hydroxyl Radicals: A Potential Source of Some Unclassified Oxygenated and Small Organosulfates in the Atmosphere

Donger Lai[1], Yanxin Bai[2], Zijing Zhang[3], Pui-Kin So[4], Yong Jie Li[5], Ying-Lung Steve Tse[6], Ying-Yeung Yeung[6], Thomas Schaefer[7], Hartmut Herrmann[7,8], Jian Zhen Yu[3,9], Yuchen Wang[2], and Man Nin Chan[1,10]

[1]Department of Earth and Environmental Sciences, Faculty of Science, The Chinese University of Hong Kong, Hong Kong, China

[2]College of Environmental Science and Engineering, Hunan University, Changsha, China

[3]Division of Environment and Sustainability, The Hong Kong University of Science and Technology, Hong Kong, China

[4]The University Research Facility in Life Sciences, The Hong Kong Polytechnic University, Hong Kong, China

[5]Department of Civil and Environmental Engineering, Department of Ocean Science and Technology, and Centre for Regional Oceans, Faculty of Science and Technology, University of Macau, Taipa, Macau SAR, China

[6]Department of Chemistry and The State Key Laboratory of Synthetic Chemistry, The Chinese University of Hong Kong, Hong Kong, China

[7]Atmospheric Chemistry Department (ACD), Leibniz Institute for Tropospheric Research (TROPOS), Leipzig, Germany

[8]School of Environmental Science and Engineering, Shandong University, Qingdao, China

[9]Department of Chemistry, The Hong Kong University of Science and Technology, Hong Kong, China

[10]The Institute of Environment, Energy, and Sustainability, The Chinese University of Hong Kong, Hong Kong, China

Correspondence to: Yuchen Wang (ywang@hnu.edu.cn) and Man Nin Chan (mnchan@cuhk.edu.hk)

Abstract

Organosulfates (OSs) are ubiquitously present in atmospheric aerosols and cloud droplets, and affect aerosol-cloud-climate interactions via their distinct physicochemical properties. Although various formation pathways and transformation mechanisms have been proposed, the origins of many atmospheric OSs remain unclear or unexplained. In this study, we investigated the aqueous-phase oxidation of an α-pinene-derived organosulfate ($C_{10}H_{17}O_5SNa$, αpOS-249) by $^{\bullet}OH$ radicals as a potential source of some uncharacterized atmospheric OSs by quantifying the kinetics and characterizing the reaction products. An aqueous-phase photoreactor was used to conduct the aqueous-phase $^{\bullet}OH$ oxidation of αpOS-249, revealing a rate constant of $(2.2 \pm 0.2) \times 10^9$ L mol^{-1} s^{-1} and atmospheric lifetimes ranged from minutes to about 2 days under atmospherically relevant cloud conditions. The product analysis revealed that a variety of more oxygenated C_{10} OS products, smaller OS ($<C_{10}$) products, and inorganic sulfates (e.g., bisulfate and sulfate) can be produced via functionalization and fragmentation processes upon oxidation. Most of the OS products have been detected in the atmosphere, with some of them whose sources and formation mechanisms are unknown thus far. Our study provides a new perspective that the chemical transformation of larger OSs via aqueous-phase oxidation can proceed efficiently to yield a variety of new OSs, serving as a source for atmospheric OSs, particularly smaller OSs. These findings would be useful in field data interpretation and model simulations regarding the abundance, formation, transformation, and atmospheric fates of OSs.

TOC
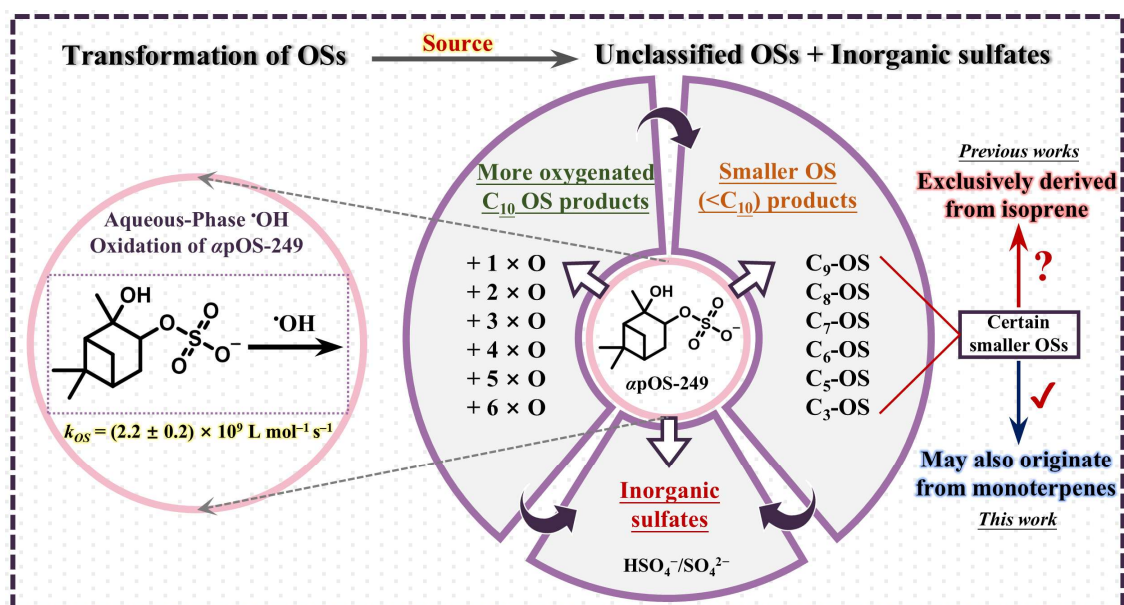
1 Introduction

Organosulfates (OSs) have been identified as ubiquitous components in secondary organic aerosol (SOA) originated from volatile organic compounds (VOCs) in the presence of sulfur species, as evidenced by laboratory studies and atmospheric observations (Surratt et al., 2007; Surratt et al., 2008; Brüggemann et al., 2020; Fan et al., 2022). OSs have also been proven to constitute a significant fraction of the organic matter of atmospheric fine particulate matter (PM2.5), contributing approximately 5–30 % (Hettiyadura et al., 2019; Chen et al., 2021; Hughes et al., 2021; Wang et al., 2022; Yang et al., 2024). In addition, atmospheric OSs possess numerous physiochemical properties including viscosity, acidity, morphology, hygroscopicity, toxicity, and surface activity, that are closely linked to their molecular structures (Hansen et al., 2015; Riva et al., 2019; Bain et al., 2023). Notably, Bain et al. (2023) demonstrated that OSs exhibit intermediate properties between inorganic sulfates (e.g., bisulfate (HSO_4^-) and sulfate (SO_4^{2-}) ions) and structurally similar alkyl organics containing functional groups other than the sulfate group (e.g., alcohols and carboxylic acids). They further reported a clear positive relationship between the carbon chain length of alkyl sulfates and surface activity. These distinctive properties ultimately govern the different environmental behaviors of OSs compared to their inorganic sulfate counterparts. Despite the potentially significant influence of aerosol physicochemical properties, the sources, formation and transformation mechanisms of OSs are still not well understood and are poorly constrained in current atmospheric model simulations (Shrivastava et al., 2017; Brüggemann et al., 2020).

Various mechanisms have been proposed for OS formation, with the acid-catalyzed ring-opening of epoxides in the presence of sulfate ions being the most widely recognized mechanism for OS formation from the photochemical reactions of various VOCs such as isoprene, monoterpenes (e.g., α-pinene, β-pinene, and limonene), and aromatic compounds (e.g., toluene and benzene) (Iinuma et al., 2007; Surratt et al., 2010; Zhang et al., 2012; Barbosa et al., 2017; Brüggemann et al., 2020; Jiang et al., 2022). In addition, heterogeneous reactions of gas-phase SO_2 with unsaturated hydrocarbons (e.g., oleic acid and linoleic acid) in the absence of gas-phase oxidant (e.g., O_3 and $^{\bullet}OH$) have been identified as another important contributor to OS formation in both laboratory experiments and field observations (Shang et al., 2016; Passananti et al., 2016; Zhu et al., 2019). Other proposed mechanisms include sulfate esterification reactions (Minerath et al., 2008; Perri et al., 2010), nucleophilic substitution of alcohols or epoxides with sulfuric acid (Surratt et al., 2007; Darer et al., 2011), and reactions facilitated by sulfoxy radicals (e.g., $SO_3^{\bullet-}$ and $SO_4^{\bullet-}$) (Nozière et al., 2010; Szmigielski, 2016; Wach et al., 2019). However, the proposed reaction mechanisms cannot fully explain the

sources, formation and composition of OSs detected in atmosphere. For instance, a review paper summarized the global overview of OS concentrations and identified various sources, including isoprene, monoterpenes, anthropogenic and unassigned sources (Brüggemann et al., 2020). The field observations revealed that OSs with unknown sources constituted 4.7 % to 99.8 % by mass in different regions (Brüggemann et al., 2020). Furthermore, a field study indicated that a significant fraction of organosulfur compounds, in particular OSs, remained unknown at the molecular level, accounting for 67 % to 79 % by mass in the eastern and western U.S. (Chen et al., 2021). These findings suggest that while hundreds of OSs have previously been identified, a significant portion of atmospheric OSs remains uncharacterized, with unknown precursors and formation mechanisms.

Additionally, the transformation of OSs after formation has also been noted in recent studies (Darer et al., 2011; Hu et al., 2011; Kwong et al., 2018; Xu et al., 2022; Ng et al., 2022; Lai et al., 2023; Xu et al., 2024; Lai et al., 2024; Lai et al., 2025). The importance of OS transformation is largely contingent upon the fate of either retaining the sulfate moiety or releasing inorganic sulfates through subsequent reactions. In the previous works on OSs (e.g., methyl sulfate, hydroxyacetone sulfate, and phenyl sulfate), aqueous-phase $^{\bullet}$OH oxidation has been shown to be an efficient removal pathway of OSs with rate constant between 10^8 to 10^9 L mol^{-1} s^{-1} (Lai et al., 2024; Gweme and Styler, 2024; Lai et al., 2025). Therefore, in this study, aqueous-phase $^{\bullet}$OH oxidation was applied to α-pinene-derived organosulfate (C$_{10}$H$_{17}$O$_5$SNa, αpOS-249, sodium 2-hydroxy-2,6,6-trimethylbicyclo[3.1.1]heptan-3-yl sulfate), a model compound of monoterpene-derived OSs. αpOS-249 is the first generation product of the $^{\bullet}$OH initiated photooxidation of α-pinene in the presence of acidic sulfate aerosols and was selected due to its global atmospheric presence (Surratt et al., 2008), with its mass ratio to total OSs ranging from 0.1 % to 17.7 % (**Table S1**) (Kristensen and Glasius, 2011; Yttri et al., 2011; Ma et al., 2014; Wang et al., 2017; Wang et al., 2018; Wang et al., 2019). Particularly, the objectives of this work are (1) to examine the kinetics of the aqueous-phase $^{\bullet}$OH oxidation of αpOS-249, (2) to identify reaction products and propose reaction mechanisms, and (3) to examine whether larger OSs can serve as precursors for smaller OSs through fragmentation processes upon oxidation.

2 Experimental methods

2.1 Aqueous-phase oxidation

The synthesis of αpOS-249 was through the monosulfation of α-pinene diol with sulfur trioxide-pyridine complex directly (Wang et al., 2017). The purity of αpOS-249 was higher

than 99 % based on nuclear magnetic resonance (NMR) spectra. Pure standard was stored in a freezer at −20 °C prior to the experiments. The experimental overview and conditions of aqueous-phase $^\bullet$OH oxidation of αpOS-249 were summarized in **Scheme S1** and **Table S2**, respectively. The experiments included kinetic experiments (αpOS-249 + reference compound (i.e., benzonic acid (BA) + $^\bullet$OH), product-capture experiments (αpOS-249 + $^\bullet$OH), and control experiments (αpOS-249 + UV light only and αpOS-249 + H_2O_2 only). All experiments were performed in a photoreactor with a volume of 150 mL (Witkowski and Gierczak, 2017; Witkowski et al., 2018; Witkowski et al., 2023; Witkowski et al., 2024). A quartz plate covered the top of the reactor and was sealed with flange clamps. The inner layer of the reactor held the reaction mixture, and circulating cooling water flowed through the outer layer to maintain a temperature of 298 ± 1 K, regulated by a refrigerated bath circulator (SD15R-30-A12E, PolyScience). The reaction mixture was continuously stirred with a magnetic stirrer to ensure homogeneity during the oxidation. A 300 W Xenon lamp (HSX-UV300, Beijing NBeT) equipped with a quartz UV filter maintained peak emission at 313 nm, which was used to generate $^\bullet$OH radicals through the photolysis of H_2O_2. The photoreactor was housed in a dark box to prevent interference from external light sources.

A typical kinetic experiment commenced (time zero) by activating the Xenon lamp to irradiate the reaction solution containing αpOS-249, BA, and H_2O_2. BA was added as a reference compound to track $^\bullet$OH. Under irradiation, a steady-state concentration of $^\bullet$OH ($[^\bullet OH]_{ss}$) of around $(4 - 9) \times 10^{-14}$ mol L^{-1} was generated, as calculated from the simulations using a box model (**Section S3**) (Witkowski and Gierczak, 2017; Otto et al., 2019). This concentration is in good agreement with previously reported $[^\bullet OH]_{ss}$ levels in cloud and fog water (Choudhary et al., 2023). The reaction progress was monitored by sampling 1.5 mL aliquots from the reactor at regular time intervals over a total duration of 3 hours (every 15 mins in the initial hour and every 30 mins in the subsequent two hours). Each sample was instantly mixed with 0.3 mL catalase solution (2 mg mL^{-1}) to decompose the residual H_2O_2 and stop further reactions (Witkowski and Gierczak, 2017; Witkowski et al., 2018). These samples were incubated at 298 K for 20 mins and then filtered through a PTFE syringe filter (45 mm, 0.2 μm pore size, Pall Corporation) before subsequent chemical analysis. The pH values of the reaction mixtures were monitored using an electrochemical meter (Orion Versastar Pro, Thermo Scientific) pre-calibrated with pH buffer solutions. The procedure for product-capture experiments was the same as the kinetic experiments, except that BA was not added. Two sets of control experiments were conducted. One involved irradiating a solution of

αpOS-249 alone to examine the effects of light only. The other set combined αpOS-249 and H_2O_2 in the dark to isolate the effects of H_2O_2.

2.2 Chemical characterization with LC-ESI-Orbitrap MS

5   The decay of αpOS-249 and BA upon oxidation was quantified by a UHPLC system (Dionex Ultimate 3000, Thermo Fisher Scientific) coupled with an Orbitrap mass spectrometer (IQ-X Tribrid, Thermo Fisher Scientific) employing calibration curves. The calibration curves were established using the synthesized αpOS-249 and commercially available BA as standards. The uncertainties in the measurements of αpOS-249 and BA were determined by the

10   reproducibility of integrated peak areas across multiple measurements at the same concentration. In addition, reaction products (e.g., OS products) formed upon oxidation were detected by the same system. Experimental details can be found in previous publications (Brüggemann et al., 2019; Wang et al., 2022). Briefly, chromatographic separation was performed by an Acquity UPLC HSS T3 column (2.1 mm × 100 mm, 1.8 μm; Waters) with a

15   gradient elution program as follow: mobile phase consisting of eluent A (H_2O with 0.1 % formic acid) and eluent B (acetonitrile with 0.1 % formic acid), at a flow rate of 0.3 mL min^{-1}. Eluent B was initially set at 5 % for 1.0 min, gradually increased to 99 % in 8.0 min, held at 99 % for 2.0 min, and then rapidly decreased back to 5 % within 0.1 min, and maintained at 5 % for the final 2.9 min, resulting in a total run time of 13.0 min. The injection volume was 3

20   μL. The Orbitrap MS detection was performed in negative electrospray ionization mode, under the following settings: spray voltage at 2300 V, sheath gas at 40 Arb, auxiliary gas at 10 Arb, sweep gas at 2 Arb, RF Lens of 30 %, ion transfer tube temperature of 300 °C, and the vaporizer temperature of 320 °C. The analysis began with a full MS scan. For MS/MS data acquisition, the MS was operated in data-dependent acquisition mode with stepped HCD collision energy

25   of 15 %, 25 %, and 40 %. The intensity threshold for triggering MS/MS data acquisition was set at 1×10^5. The MS resolution was configured to 120,000 and 30,000 for full MS scan and MS/MS scan, respectively. The m/z range for the full MS scan was 50−1200 and 50−500 for the MS/MS scan. The data were analyzed using Xcalibur (version 4.1) as well as the open-source software package MZmine 2.38, following the workflows and methods previously

30   described (Brüggemann et al., 2019; Wang et al., 2022).

2.3 Quantification of inorganic sulfates with Ion Chromatography

The formation of inorganic sulfates (HSO_4^-/SO_4^{2-}) during the aqueous $^\bullet OH$ oxidation of αpOS-249 was determined using ion chromatography (IC). The details have been given in previous studies (Xu et al., 2022; Lai et al., 2023). Briefly, the samples were analyzed with a Dionex ICS-1100 IC system (Thermo Fisher Scientific). Inorganic sulfate anions were separated using an IonPac AS11-HC analytical column (4 mm × 250 mm) and an IonPac AG11-HC guard column (4 mm × 50 mm). The IC system operated in negative mode with 15 mmol L^{-1} NaOH as the eluent at a flow rate of 0.8 mL min^{-1}. Moreover, the concentration of SO_4^{2-} anions quantified by IC represents the total amount of HSO_4^- and SO_4^{2-} (Xu et al., 2022; Lai et al., 2023). In this work, the quantity of inorganic sulfates was measured based on its peak area in the chromatogram and quantified using a calibration curve based on Na_2SO_4 standard, with a retention time (RT) of 4.0 min. The uncertainty of inorganic sulfate measurements was found to be 2.5 % from repeated measurements.

3 Results and discussion

3.1 Oxidation kinetics

Control experiments were conducted to account for any non $^\bullet OH$ losses, including αpOS-249 photolysis due to UV radiation alone and the reaction of αpOS-249 with H_2O_2 in the absence of light (**Section S4**). **Figure S1** reveals that αpOS-249 neither photolyzes nor reacts with H_2O_2 unless light is present to generate $^\bullet OH$. Furthermore, as discussed in **Section S5**, the aqueous-phase $^\bullet OH$ oxidation kinetics of αpOS-249 is likely insensitive to solution pH under typical atmospheric conditions.

Relative rate method was adopted to determine the second-order rate constants for $^\bullet OH$ oxidation of αpOS-249 (k_{OS}) by comparing the measured rate constants to that of a reference compound (BA) with a well-known $^\bullet OH$ reaction rate of $k_{Ref} = (5.5 \pm 0.3) \times 10^9$ L mol^{-1} s^{-1} at a solution pH of 4.5 (Hems and Abbatt, 2018), a condition that is the same as our experiments (**Section S5**). In the reaction mixture, $^\bullet OH$ reacts with both αpOS-249 (**R1**) and BA (**R2**) as described in the reactions shown below (Hems and Abbatt, 2018). The second-order rate constants for the $^\bullet OH$ oxidation of αpOS-249 (k_{OS}) were calculated using **Eqn. 1**, where [αpOS-249] and [BA] are the concentrations of αpOS-249 and BA, respectively, at the initial (time = 0) and intermediate (time = t) time:

$$^\bullet OH + \alpha pOS\text{-}249 \xrightarrow{k_{OS}} \text{products} \tag{R1}$$

$$^\bullet OH + BA \xrightarrow{k_{Ref}} \text{products} \tag{R2}$$
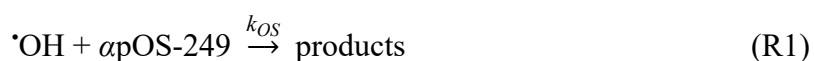
$$\ln \left(\frac{[\alpha pOS\text{-}249]_0}{[\alpha pOS\text{-}249]_t}\right) = \frac{k_{OS}}{k_{Ref}} \ln \left(\frac{[BA]_0}{[BA]_t}\right) \qquad \text{(Eqn. 1)}$$

Figure 1 (a) illustrates the relative kinetic plot, yielding a k_{OS} value of $(2.2 \pm 0.2) \times 10^9$ L mol^{-1} s^{-1} at 298 K. The uncertainty of k_{OS} was calculated by propagating the two standard deviations (2σ) from multiple experiments, the reported uncertainty of the rate constant for the reference compound, and the uncertainties from measurements of $\alpha pOS\text{-}249$ and BA (Witkowski and Gierczak, 2017). The rate constant is compared with that predicted by the structure-activity relationship (SAR) model which has been widely used to estimate the reactivity of various organic compounds towards ${}^\bullet$OH radicals in aqueous phase (Monod and Doussin, 2008; Doussin and Monod, 2013). Our recent laboratory work revealed the strong deactivating effect of the sulfate group ($-OSO_3{}^-$) on aqueous-phase ${}^\bullet$OH radicals oxidation kinetics, and extended the SAR model to include OSs (Lai et al., 2024), by introducing new interaction parameters for the $-OSO_3{}^-$ group (F (α-position) $= 0.22$ and G (β-position) $= 0.44$). Here, we predicted the second-order rate constant for the aqueous-phase ${}^\bullet$OH oxidation of $\alpha pOS\text{-}249$ to be 3.1×10^9 L mol^{-1} s^{-1} (**Section S6** and **Figure S2**), which is higher than our measured value of $(2.2 \pm 0.2) \times 10^9$ L mol^{-1} s^{-1}. This difference is within an acceptable range when considering the performance of the SAR model (58 % of simulated rates within $\pm$ 20 % and 76 % within $\pm$ 40 % of experimental data) (Monod and Doussin, 2008; Doussin and Monod, 2013). This suggests that the SAR model is a valuable tool for predicting the aqueous-phase ${}^\bullet$OH oxidation rate constants of a variety of atmospheric OSs.

We also assessed the significance of aqueous-phase ${}^\bullet$OH oxidation in its atmospheric fate by estimating the atmospheric lifetimes (**Figure 1 (b)**), $\tau = 1/(k_{OS} \times [{}^\bullet OH])$ (Wen et al., 2021). The estimated lifetimes based on the newly obtained experimental data varied from approximately 3 mins in remote aerosol conditions ($[{}^\bullet OH] = 3 \times 10^{-12}$ mol L^{-1}) to about 2 days in urban cloud conditions ($[{}^\bullet OH] = 3.5 \times 10^{-15}$ mol L^{-1}) (Herrmann et al., 2010). In addition, using SAR predictions with higher rate constant yield shorter lifetimes, ranging from about 2 mins in remote aerosol conditions to about 1 day in urban cloud conditions. Given these relatively short atmospheric lifetimes, the aqueous-phase ${}^\bullet$OH oxidation could likely serve as a significant transformation pathway for $\alpha pOS\text{-}249$.
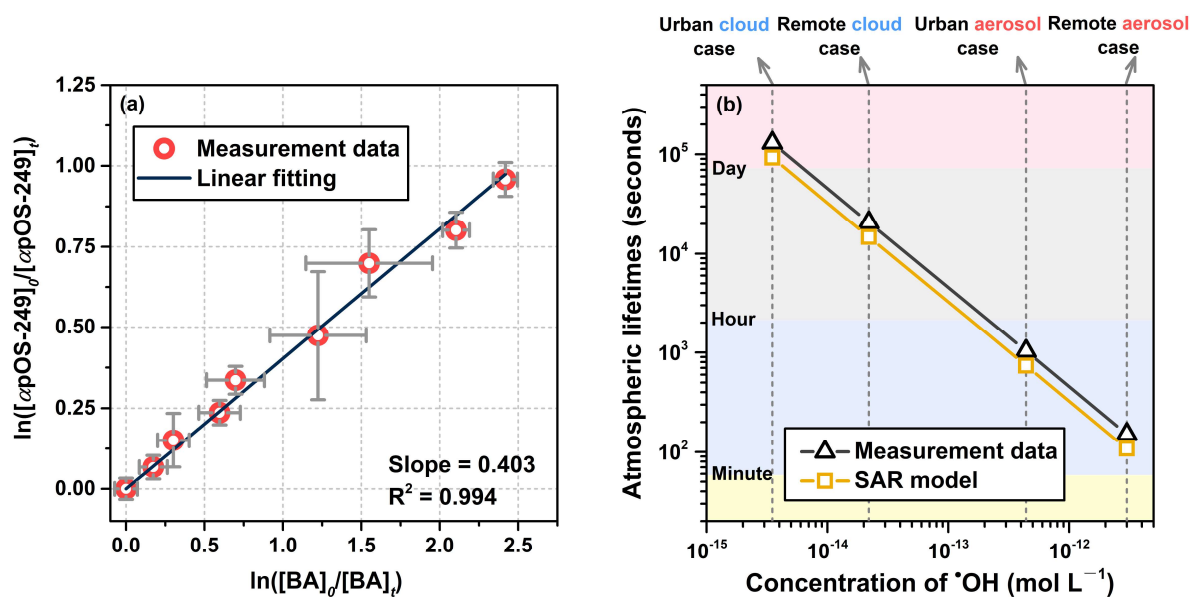
Figure 1. (a) Relative kinetic plot of aqueous-phase $^{\bullet}$OH oxidation of αpOS-249 in accordance with **Eqn. 1** using benzoic acid as the reference compound. (b) Atmospheric lifetimes of αpOS-249 against the aqueous-phase $^{\bullet}$OH oxidation was calculated under various scenarios using rate constant obtained from this study (measurement data) and the SAR model. The concentrations of $^{\bullet}$OH in the aqueous phase under four different scenarios were obtained from the modeling study (Herrmann et al., 2010).

3.2. Oxidation products formed upon oxidation

Figure S3 shows the total ion chromatograms (TICs) obtained from the product-capture experiments. Before oxidation (**Figure S3 (a)**, t_0), a dominant peak corresponding to the [M–H]$^-$ ion of αpOS-249 (m/z = 249.08, C$_{10}$H$_{17}$O$_5$S$^-$) is observed at a retention time (RT) of 4.7 min. After 45 mins of $^{\bullet}$OH oxidation (**Figure S3 (b)**, t_{45}), the intensity of αpOS-249 significantly decreases, accompanied by the emergence of new product peaks with low intensities. After 3 hours of oxidation (**Figure S3 (c)**, t_{180}), αpOS-249 is almost completely consumed. Notably, some new product peaks observed at t_{45} exhibit a declining trend, suggesting their susceptibility to $^{\bullet}$OH oxidation. A number of new OS products were detected based on two primary criteria: i) their absence prior to oxidation (t_0), and ii) the presence of fragmentation patterns in their MS^2 spectra, primarily showing the bisulfate anion (HSO$_4^-$, m/z = 96.96), and often accompanied by other sulfur-containing ions such as the sulfite ion radical (SO$_3^{\bullet-}$, m/z = 79.96), and bisulfite anion (HSO$_3^-$, m/z = 80.97) (Surratt et al., 2008; Huang et al., 2018; Xu et al., 2022). These identified OS products were summarized in **Table S5** and were grouped into two categories: more oxygenated C$_{10}$ OS products, formed through

functionalization processes via the addition of oxygenated functional groups, and smaller OS ($<C_{10}$) products, which result from fragmentation processes.

Figure 2 (a) shows the time-dependent evolution of intensities for more oxygenated C_{10} OS products from different generations. These products were grouped according to the number of added oxygen atoms (e.g., $+ 1 \times O$, $+ 2 \times O$, etc). The highest intensity of first-generation products ($+ 1 \times O$) peaked at 45 mins into the reaction, followed by a noticeable decrease, while the second-generation products ($+ 2 \times O$) showed a gradual increase, lagged their peak at 90 mins before gradually declining. Third ($+ 3 \times O$) and fourth-generation ($+ 4 \times O$) products followed a similar pattern, with a relatively lower intensity compared to the first and second-generation products. They showed a slow increase, peaking at 120 mins with a minimal decrease. Additionally, fifth-generation ($+ 5 \times O$) products had even lower intensity, peaking at 150 mins, while sixth-generation ($+ 6 \times O$) products showed the lowest intensity and a continued slow increasing trend. This evolution pattern can be well described as multi-generation sequential oxygenation processes (Kroll et al., 2015).

The intensities of smaller OS ($< C_{10}$) products are categorized by their carbon atoms (e.g., C_9, C_8, C_7 etc), and their time-dependent evolutions are shown in **Figure 2 (b)**. C_9 OS products show the highest intensity, peaking at 120 mins before a slight decrease. Meanwhile, C_7 OS products show the second highest intensity, but significantly lower than C_9 OS products, displaying a consistent upward trend. The other OS groups all demonstrate a continued increasing trend with low intensities. Unlike more oxygenated C_{10} OS products, the evolution of smaller OS products always keep increasing with reaction time, suggesting that fragmentation likely begins to gain increased significance as oxidation proceeds.
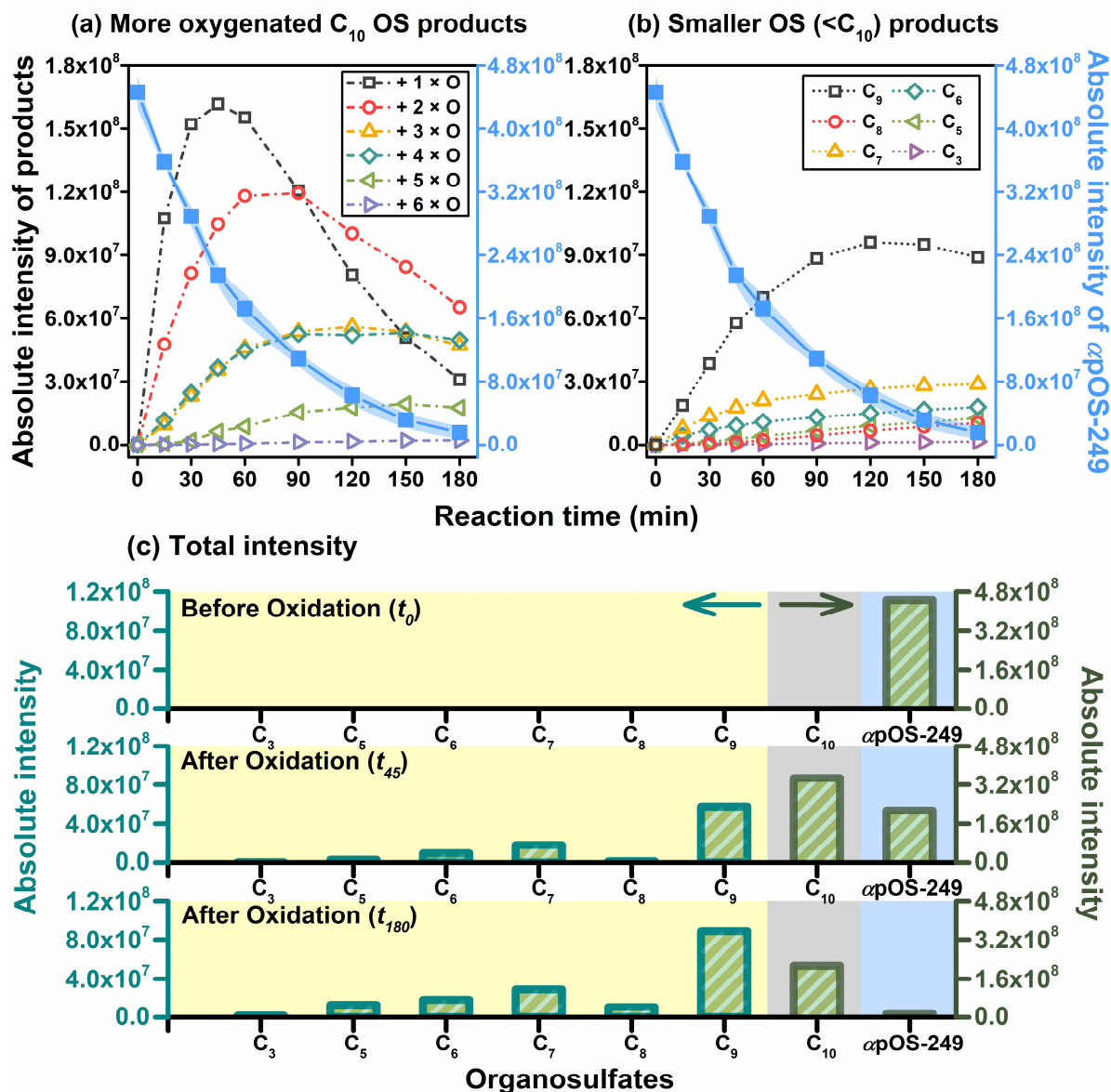
Figure 2. Time-dependent evolution of absolute intensities for αpOS-249 decay and reaction products formed during the aqueous-phase ·OH oxidation of αpOS-249, (a) more oxygenated C_{10} OS products, (b) smaller OS ($<C_{10}$) products, and (c) total intensity.

Figure 2 (c) shows the variation in absolute intensity of αpOS-249 and its oxidation products with different carbon atoms before (t_0) and after (t_{45} and t_{180}) oxidation. The total intensity of C_{10} OS products initially exhibits a significant increase followed by a decline. Meanwhile, the intensity of smaller OS ($<C_{10}$) products steadily increases throughout the reaction. This implies that functionalization processes likely dominate over the fragmentation processes in the early oxidation stages (e.g., within the initial hour). However, as oxidation proceeds, fragmentation processes begin to gain comparable significance (**Figure S4**). It is

important to note that this simple comparison assumes that OS products have the same ionization efficiency as αpOS-249. However, differences in ionization efficiency among OS products relative to the parent OS are not well understood. As a result, the findings from this simple analysis should be interpreted with caution. Authentic standards are important for accurately quantifying more oxygenated C_{10} OS products and smaller OS products. In the absence of these standards, quantification becomes challenging, and both overestimation and underestimation are possible depending on the specific molecular structures involved. Furthermore, this observed trend agrees with the hypothesis that as oxidation continues, the addition of functional groups to the parent compound increases, leading to a higher probability of alkoxy radicals' formation with functional groups on the β-carbon (Kroll et al., 2011; Kessler et al., 2012; Lambe et al., 2012; Wiegel et al., 2015; Hems and Abbatt, 2018; Jiang et al., 2023). This, in turn, enhances the fragmentation processes, as the addition of oxygenated functional groups on the β-carbon plays an activating role and reduces the energy barrier for decomposition (Wiegel et al., 2015). Furthermore, other factors such as higher O/C ratios and increased polarity can enhance the alkoxy decomposition, thereby favoring the fragmentation process at later stages of oxidation (Wiegel et al., 2015).

3.3 Reaction mechanisms

Upon oxidation, the ˙OH radical can initially attack different reaction sites. **Table S4** and **Figure S2** show the partial rate constants for hydrogen abstraction at various reaction sites, as derived from the SAR model. The model predicts that the relative reactivity ranges from 2.3 % at 5-C to 21.2 % at 3-C. ˙OH radicals do not exhibit an overall strong preference for specific carbon types (primary carbons: 34.8 %, secondary carbons: 29.7 %, and tertiary carbons: 32.6 %) (**Table S4**). For simplicity and clarity, we proposed the mechanisms involving the three types of carbon atoms with the highest predicted partial rate constants in **Scheme 1**. A generic reaction scheme outlining the formation of the identified OS products was shown in **Scheme S2**, based on well-established reaction pathways reported in the literatures (Russell, 1957; Bennett and Summers, 1974; Hearn et al., 2007; Smith et al., 2009; George and Abbatt, 2010; Kroll et al., 2015).
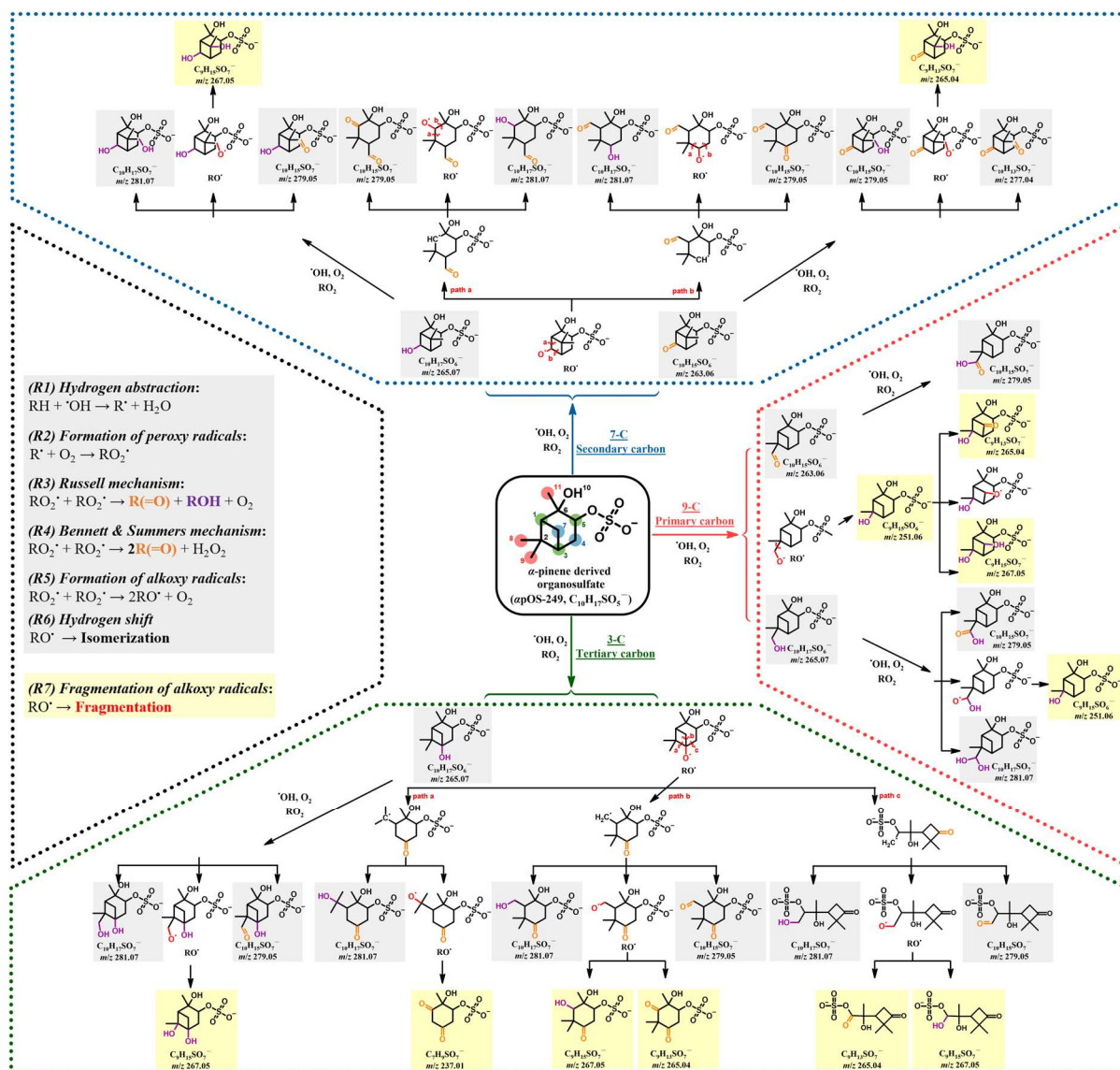
Scheme 1. Proposed mechanisms for the formation of C_{10} OS products and smaller OS ($<C_{10}$) products through functionalization and fragmentation processes during the aqueous-phase $^{\bullet}$OH oxidation of αpOS-249, using 3-C, 7-C, and 9-C as representative examples with the highest predicted partial rate constants (For simplicity and clarity, we only proposed the mechanisms up to the second-generation products). Grey and yellow base colours distinguish the C_{10} OS products and smaller OS products, respectively.

3.3.1 C_{10} OS products

As shown in **Scheme 1** and **Table S5**, a number of more-oxygenated C_{10} OS products were detected during oxidation, likely formed through functionalization processes. These processes initiate with hydrogen abstraction by $^{\bullet}$OH radicals from αpOS-249, leading to the formation of an alkyl radical (R$^{\bullet}$). The alkyl radicals then rapidly combine with O_2 to yield peroxyl radical (RO$_2^{\bullet}$). The subsequent self-reactions of RO$_2^{\bullet}$ could lead to the formation of

diverse products, incorporating oxygenated functional groups (e.g., hydroxyl (−OH), and carbonyl (=O) groups) into the parent molecule (i.e., αpOS-249) without breaking the C-C bonds (Kroll et al., 2009; Lambe et al., 2012). Generally, the addition of n number of oxygenated functional groups to αpOS-249 represents the nth generation of oxygenation (Wilson et al., 2012; Ng et al., 2022). For example, as shown in **Scheme 1**, first-generation products are formed by adding either one hydroxyl group or one carbonyl to αpOS-249, yielding compounds such as $C_{10}H_{17}SO_6^-$ ($m/z = 265.07$) and $C_{10}H_{15}SO_6^-$ ($m/z = 263.06$). These OS products show an increase of one oxygen atom ($+ 1 \times O$) compared to the parent compound. Different structural isomers of $C_{10}H_{17}SO_6^-$ and $C_{10}H_{15}SO_6^-$ can be formed depending on different initial reaction sites. The presence of multiple peaks with different retention times during LC-MS analysis for a given OS ion supports the presence of the isomeric products **(Table S5)**.

Upon oxidation, first-generation products can transform into second-generation products. These second-generation products arise from the addition of an extra oxygen atom, continually incorporating carbonyl or hydroxyl groups into the first-generation products, thereby adding two oxygen atoms to the parent compound ($+ 2 \times O$). Three combinations of this transformation are possible: the addition of two hydroxyl groups, one carbonyl and one hydroxyl group, or two carbonyl groups. For example, as shown in **Scheme 1**, $C_{10}H_{17}SO_7^-$ ($m/z = 281.07$) represents the first case through the addition of two hydroxyl groups. $C_{10}H_{15}SO_7^-$ ($m/z = 279.05$) represents the second case, formed by incorporating both carbonyl and hydroxyl groups into parent compound. This compound can result from carbonyl addition to first-generation hydroxyl products, or hydroxyl addition to first-generation carbonyl products. Lastly, $C_{10}H_{13}SO_7^-$ ($m/z = 277.04$) represents the third case, involving the addition of two carbonyl groups. Furthermore, the progression towards more oxygenated C_{10} OS products can be sustained, enabling the continual incorporation of new functional groups into parent compound. Among the identified OS products (**Table S5**), the most oxygenated C_{10} OS products were found to be $C_{10}H_{15}SO_{11}^-$ ($m/z = 343.03$), inferring the addition of six oxygenated functional groups.

3.3.2 Smaller OS ($<C_{10}$) products

Smaller OS ($<C_{10}$) products were also detected, ranging from C_3 to C_9 OS products. Detailed molecular information about these OS products is summarized in **Table S5**. Unlike more oxygenated C_{10} OS products, the formation of fragmentation products is likely occurred through multiple pathways across various oxidation generations. For simplicity, we proposed

in **Scheme 1** several possible mechanisms, involving three specific carbon atom types and focusing on RO$^{\bullet}$ decomposition through C-C bond scission (George and Abbatt, 2010).

Upon oxidation, the fragmentation processes initiate with the same mechanisms as the functionalization processes until the alkoxy radicals (RO$^{\bullet}$) form following the self-reactions of RO$_2$$^{\bullet}$. For example, for tertiary carbon 3-C, with the highest partial rate constant, three scission pathways (path a, b, and c, **Scheme 1**) from RO$^{\bullet}$ radicals generate smaller OS products such as C$_7$H$_9$SO$_7$$^-$ ($m/z = 237.01$), C$_9$H$_{15}$SO$_7$$^-$ ($m/z = 267.05$), and C$_9$H$_{13}$SO$_7$$^-$ ($m/z = 265.04$). These C$_9$ OS products can also be formed during initial hydrogen abstraction from primary (9-C) and secondary carbon sites (7-C) with different structures. We acknowledge that various reaction pathways can potentially lead to the same smaller OS products, with **Scheme 1** outlining certain possible pathways. For example, C$_9$H$_{15}$SO$_6$$^-$ ($m/z = 251.06$) could originate from the decomposition of RO$^{\bullet}$ following initial hydrogen abstraction from the primary (9-C) carbon site or from the subsequent oxidation of C$_{10}$H$_{17}$SO$_6$$^-$ ($m/z = 265.07$).

3.3.3 Inorganic sulfates

Previous studies on the heterogeneous $^{\bullet}$OH oxidation of various OSs, involving aliphatic, isoprene-derived, and pinene-derived OSs, have reported the formation of inorganic sulfates (e.g., HSO$_4$$^-$ and SO$_4$$^{2-}$) (Kwong et al., 2018; Chen et al., 2020; Xu et al., 2022). We also investigated the significance of this conversion from organosulfur in αpOS-249 to inorganic sulfur upon aqueous-phase $^{\bullet}$OH oxidation (**Section S10**). **Figure S5** shows the ion chromatograms before (t_0) and after (t_{45} and t_{180}) aqueous-phase $^{\bullet}$OH oxidation of αpOS-249. Before oxidation, a minor presence of inorganic sulfates (3.2 ± 0.1 % of total sulfur molar) was detected, likely due to αpOS-249 hydrolysis (**Figure S5**) (Xu et al., 2022). This amount has been corrected for the quantification of inorganic sulfate formed upon oxidation. After oxidation (**Figure S5**), a continued increase in the inorganic sulfate signal was observed. This inorganic sulfate formation was not detected in any control experiments and inferring that it is formed during aqueous-phase $^{\bullet}$OH oxidation of αpOS-249. **Figure 3** shows the temporal evolution of αpOS-249 and inorganic sulfate (HSO$_4$$^-$ and SO$_4$$^{2-}$) concentrations during the aqueous-phase $^{\bullet}$OH oxidation of αpOS-249. Over the 3-hour oxidation period, αpOS-249 was nearly full consumed, while inorganic sulfate concentration steadily increased. The inorganic sulfate yield, calculated as the moles of inorganic sulfate formed per mole of αpOS-249 reacted over reaction time, reached of 46 ± 2 % at the end of experiment (**Figure S6**). These results suggest that within the timeframe of aqueous-phase $^{\bullet}$OH oxidation, about half of the sulfur in reacted αpOS-249 upon oxidation was converted to inorganic sulfate. We anticipate a

continuous increase in inorganic sulfate concentration when the reaction further proceeds. Future work is warranted regarding the dependence of inorganic sulfate formation on the extent of OS oxidation in the atmosphere.
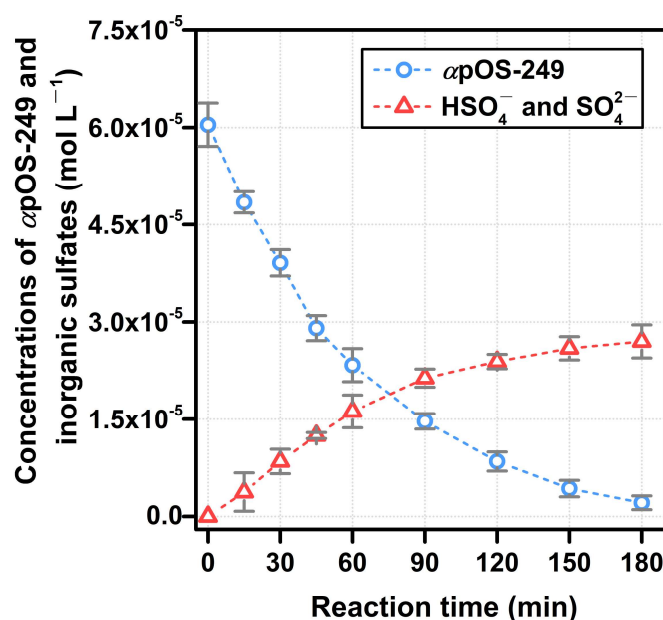
Figure 3. Concentrations of αpOS-249 and inorganic sulfates (HSO$_4^-$ and SO$_4^{2-}$) as function of reaction time during the aqueous-phase $^\bullet$OH oxidation of αpOS-249.

Upon oxidation, the generation of inorganic sulfates involves the formation and reactions

10   of sulfate radical anion (SO$_4^{\bullet-}$) (Ng and Chan, 2023). This sulfur radical species is likely derived from the cleavage of C-O bond, occurring when a RO$^\bullet$ is created with the $-$O$^\bullet$ situated at the β position of the $-$OSO$_3^-$ group (Ng and Chan, 2023). In the presence of H$_2$O, SO$_4^{\bullet-}$ can subsequently converted into HSO$_4^-$, which can exist in equilibrium with SO$_4^{2-}$. Both HSO$_4^-$ and SO$_4^{2-}$ contribute the yield of inorganic sulfates (Lai et al., 2023). Based on SAR predictions

15   (**Figure S2**), hydrogen abstraction at the α-position 5-C reaction site, leading to the direct formation of SO$_4^{\bullet-}$, shows the lowest relative reactivity (2.3 %) compared to other sites. This small reactivity can be explained by the electron-withdrawing nature of $-$OSO$_3^-$ groups, which lower the electron density of the α C$-$H bond and decrease the rate of hydrogen abstraction (Berruti et al., 2022; Lai et al., 2024). Considering this low reactivity, the generation of SO$_4^{\bullet-}$

20   through C-O bond cleavage in the 5-C alkoxy radical directly from αpOS-249, and its subsequent conversion to inorganic sulfates (**Scheme S3**), may not be a favorable reaction pathway.

Possible explanations the sulfur conversion from αpOS-249 to inorganic sulfate could be: 1) enhanced likelihood of α-position alkoxy radical decomposition to $SO_4^{\bullet-}$ as oxidation proceeds, altering site selectivity of $^{\bullet}OH$ hydrogen abstraction when more oxygenated and functional groups are added to the carbon backbone (e.g., different generations of oxygenated C_{10} OS products), 2) increased production of smaller OS products leading to easier C-O bond cleavage and inorganic sulfate formation due to fewer carbon atoms, 3) in addition to $SO_4^{\bullet-}$ pathway, the formation of inorganic sulfates may also occur through the non-$SO_4^{\bullet-}$ reaction pathway. For example, a recent laboratory study proposed an alternative mechanism for inorganic sulfate formation, suggesting the involvement of sulfite radical anion ($SO_3^{\bullet-}$) from the cleavage of (C)O−S bonds, triggering a series of chain reactions resulting in inorganic sulfate formation (Xu et al., 2024), and 4) when oxidation proceeds, more tertiary OS products are likely produced. This could increase the possibility of inorganic sulfates formed from the hydrolysis of these tertiary OS products. For instance, the efficient hydrolysis can occur for certain tertiary OSs, such as isoprene-derived OSs, under relevant ambient acidities (Hu et al., 2011). Further studies are warranted to better understand the role of hydrolysis in OS transformation.

It is important to note that the formation of $SO_4^{\bullet-}$ via C-O bond cleavage in $RO^{\bullet}$ can also lead to the formation of non-sulfated products (Xu et al., 2022). For example, C_{10} products such as $C_{10}H_{18}O_2$ ($m/z = 170.13$) and $C_{10}H_{16}O_2$ ($m/z = 168.12$) can be formed (**Scheme S3**). Their predicted Henry's law constants, calculated using HENRYWIN through the bond contribution method (Mackay and Shiu, 1981), are 4.08×10^3 M atm^{-1} and 9.17×10^1 M atm^{-1}, respectively. These predicted values are lower than that of αpOS-249 (1.35×10^9 M atm^{-1}). Given their low solubilities, these two non-sulfated products are likely partition to the gas phase and have not been detected in our product analysis. Additionally, some non-volatile products could be formed. For instance, $C_9H_{16}O_4$ ($m/z = 188.10$) and $C_9H_{14}O_4$ ($m/z = 186.09$) can be produced alongside $SO_4^{\bullet-}$ (**Scheme S3**), with predicted Henry's law constants are 1.71×10^8 M atm^{-1} and 9.52×10^6 M atm^{-1}, respectively, about one to two orders of magnitude lower than αpOS-249 (Mackay and Shiu, 1981). Among these two products, $C_9H_{14}O_4$ ($m/z = 186.09$) was detected in our product analysis, but $C_9H_{16}O_4$ ($m/z = 188.10$) was not identified.

4 Atmospheric implications

We would like to note that as shown in **Table 1** and **Table S5**, 34 out of 40 OS products formed upon aqueous-phase $^{\bullet}OH$ oxidation of αpOS-249 have been detected in ambient samples with significant atmospheric abundance. Among the detected OS products, the most

prevalent OS product, $C_5H_7SO_7^-$ ($m/z = 210.99$), has been observed at concentrations up to 131 ng m^{-3} and was previously thought to originate primarily from isoprene (**Table S5**) (Hettiyadura et al., 2019). Our findings also suggest that this OS product could also originated from the aqueous-phase $^{\bullet}$OH oxidation of αpOS-249. This can also apply to other smaller OSs

5   (<C$_{10}$), including $C_3H_5SO_5^-$, $C_7H_9SO_7^-$, and $C_8H_{11}SO_7^-$ (**Table 1**), previously linked to isoprene as a precursor. This finding also addresses that some atmospheric smaller OSs can also originate from the transformation of larger OSs (e.g., αpOS-249), particularly in the regions where the monoterpene emissions are significant. More importantly, among the identified OS products, 13 out of 40 OS products have unknown sources and 20 out of 40 OS

10   products have unknown formation pathways (**Table 1**), suggesting that the aqueous $^{\bullet}$OH oxidation of αpOS-249 could be a previously unrecognized formation pathway of these ambient-detected OSs (**Figure S7**).

Table 1. Overview of detected OS products upon the aqueous $^{\bullet}$OH oxidation of αpOS-249

15   (identified in previous studies along with suggested precursors and formation pathways).

Formula	Previous studies			This work	
	Suggested precursor	Suggested formation pathway	Ref.	Additional formation pathway	Suggested new formation pathway
Smaller OS (<C$_{10}$) products					
$C_3H_5SO_5^-$	Isoprene/glycolaldehyde/ hydroxyacetone	Isoprene + $^{\bullet}$OH + (NO) + acidic/neutral sulfate seed	(Surratt et al., 2008)	✓	
$C_5H_7SO_7^-$	Isoprene	Isoprene + $^{\bullet}$OH + acidic sulfate seed	(Surratt et al., 2008)	✓	
$C_6H_9SO_6^-$	Anthropogenic	**Unknown**	(Hettiyadura et al., 2019)		✓
$C_6H_7SO_7^-$	**Unknown**	**Unknown**	–		✓
$C_6H_9SO_8^-$	**Unknown**	**Unknown**	–		✓
$C_7H_9SO_7^-$	Isoprene	Methyl vinyl ketone + SO$_4^{\bullet-}$	(Nozière et al., 2010)	✓	
$C_7H_9SO_8^-$	**Unknown**	**Unknown**	–		✓
$C_7H_{11}SO_8^-$	**Unknown**	**Unknown**	–		✓
$C_7H_{11}SO_9^-$	**Unknown**	**Unknown**	–		✓
$C_7H_{11}SO_{10}^-$	**Unknown**	**Unknown**	–		✓
$C_8H_9SO_6^-$	**Unknown**	**Unknown**	–		✓
$C_8H_{11}SO_7^-$	Isoprene	Methyl vinyl ketone/methacrolein + SO$_4^{\bullet-}$	(Hettiyadura et al., 2019; Nozière et al., 2010; Schindelka et al., 2013)	✓	
$C_8H_{11}SO_8^-$	**Unknown**	**Unknown**	–		✓
$C_8H_{11}SO_9^-$	**Unknown**	**Unknown**	–		✓

Formula	Suggested precursor	Suggested formation pathway	Ref.	Additional formation pathway	Suggested new formation pathway
$C_9H_{15}SO_5^-$	Monoterpenes	**Unknown**	(Brüggemann et al., 2019)		✓
$C_9H_{13}SO_6^-$	Monoterpenes	Limonene/terpinolene + $^\cdot$OH + NO + highly acidic sulfate seed	(Surratt et al., 2008)	✓	
$C_9H_{15}SO_6^-$	Monoterpenes/sesquiterpenes	limonene + $^\cdot$OH + (NO) + (highly) acidic sulfate seed	(Surratt et al., 2008)	✓	
$C_9H_{11}SO_7^-$	Monoterpenes	**Unknown**	(Brüggemann et al., 2019)		✓
$C_9H_{13}SO_7^-$	Monoterpenes	**Unknown**	(Brüggemann et al., 2019)		✓
$C_9H_{15}SO_7^-$	Isoprene/monoterpenes/ anthropogenic	limonene + $^\cdot$OH + NO + highly acidic sulfate seed	(Surratt et al., 2008)	✓	
$C_9H_{13}SO_8^-$	Monoterpenes	**Unknown**	(Brüggemann et al., 2019)		✓
$C_9H_{15}SO_8^-$	Monoterpenes	α-terpinene + $^\cdot$OH + NO + highly acidic sulfate seed	(Surratt et al., 2008)	✓	
	Previous studies			**This work**	
Formula	**Suggested precursor**	**Suggested formation pathway**	**Ref.**	**Additional formation pathway**	**Suggested new formation pathway**
More oxygenated C_{10} OS products					
$C_{10}H_{15}SO_5^-$	Monoterpenes	α-pinene + $^\cdot$OH/NO$_3^\cdot$ + highly acidic sulfate seed	(Surratt et al., 2008)	✓	
$C_{10}H_{15}SO_6^-$	Monoterpenes	β-pinene + $^\cdot$OH + NO + highly acidic sulfate seed	(Surratt et al., 2008)	✓	
$C_{10}H_{17}SO_6^-$	Monoterpenes/anthropogenic	α-pinene/α-terpinene/terpinolene + $^\cdot$OH + (NO) + (highly) acidic sulfate seed	(Surratt et al., 2008)	✓	
$C_{10}H_{13}SO_7^-$	**Unknown**	**Unknown**	−		✓
$C_{10}H_{15}SO_7^-$	Monoterpenes/anthropogenic	α-pinene/β-pinene/limonene/α-terpinene/γ-terpinene + $^\cdot$OH/NO$_3^\cdot$/SO$_4^{\cdot-}$ + (NO) + (highly) acidic sulfate seed	(Surratt et al., 2008; Nozière et al., 2010)	✓	
$C_{10}H_{17}SO_7^-$	Monoterpenes	α-pinene/β-pinene /limonene/α-terpinene/terpinolene + $^\cdot$OH/SO$_4^{\cdot-}$ + (NO) + (highly) acidic sulfate seed	(Surratt et al., 2008; Nozière et al., 2010)	✓	
$C_{10}H_{13}SO_8^-$	**Unknown**	**Unknown**	−		✓
$C_{10}H_{15}SO_8^-$	Monoterpenes/anthropogenic	**Unknown**	(Brüggemann et al., 2019; Riva et al., 2016)		✓
$C_{10}H_{17}SO_8^-$	Monoterpenes/anthropogenic	α-pinene/α-terpinene/terpinolene + $^\cdot$OH/SO$_4^{\cdot-}$ + (NO) + (highly) acidic sulfate seed	(Surratt et al., 2008; Nozière et al., 2010)	✓	
$C_{10}H_{13}SO_9^-$	Monoterpenes	**Unknown**	(Brüggemann et al., 2019)		✓
$C_{10}H_{15}SO_9^-$	**Unknown**	**Unknown**	−		✓
$C_{10}H_{15}SO_{10}^-$	**Unknown**	**Unknown**	−		✓

Furthermore, the chemical aging of αpOS-249 during aqueous-phase $^\cdot$OH experiments can significantly modify the composition and physiochemical properties of atmospheric aerosols and cloud droplets. For example, $^\cdot$OH oxidation of αpOS-249 promotes the formation

of inorganic sulfates, which can enhance acidity. It also produces smaller OS products that may reduce surface activity compared with their parent αpOS-249 and larger OSs. These insights are critical for accurately evaluating the role of such atmospherically important organosulfur compounds in aerosol–cloud interactions and their potential climate impacts.

5 Conclusions

Overall, the aqueous-phase ·OH oxidation can serve as an important sink for αpOS-249 with corresponding atmospheric lifetimes ranged from minutes to about 2 days under relevant atmospheric cloud conditions. This efficient oxidation also highlights that the atmospheric abundance of αpOS-249 and potentially other structurally similar OSs (e.g., limonene derived OSs) in field studies may be underestimated if their transformation pathways are not properly considered. Moreover, aqueous-phase ·OH oxidation of αpOS-249 can yield a number of more-oxygenated C_{10} OS products, smaller OS (<C_{10}) products, and inorganic sulfates (e.g., bisulfate (HSO_4^-) and sulfate (SO_4^{2-})). Among these products, most of the OS products have been detected in the atmosphere, with some having previously unknown sources and formation mechanisms. Altogether, this study shows that the transformation pathways of OSs (e.g., αpOS-249) via aqueous-phase ·OH oxidation can serve as sources for some unclassified OSs in the atmosphere.

Data availability. Data are available upon request from the corresponding author.

Supplement. The supplement related to this article is published alongside this manuscript.

Author contributions. DL and MNC designed the experiments. DL ran the experiments. YB and YW synthesized αpOS-249 standard. ZZ and PKS helped with the chemical analysis. DL, YW, and MNC prepared the manuscript. YJL, YLST, YYY, TS, HH, and JZY provided valuable comments and suggestions for the manuscript.

Competing interests. The contact author has declared that none of the authors has any competing interests.

Disclaimer. Publisher's note: Copernicus Publications remains neutral with regard to jurisdictional claims made in the text, published maps, institutional affiliations, or any other

geographical representation in this paper. While Copernicus Publications makes every effort to include appropriate place names, the final responsibility lies with the authors.

Acknowledgements. The authors are grateful for the financial support.

Financial support. This work is supported by The Hong Kong Research Grants Council (Ref No. 14300921: Project ID 2130791 and No. 14301922: Project ID 2130809). YW would like to acknowledge financial support by the National Nature Science Foundation of China (NSFC) (Grants 22306059), Science and Technology Innovation Program of Hunan Province (Grants 2024RC3106), and the Fundamental Research Funds for the Central Universities (Grant 531118010830). YJL acknowledges funding support from the Science and Technology Development Fund, Macau SAR (File No. FDCT 0031/2023/AFJ and No. FDCT 0107/2023/RIA2), and a multiyear research grant (File No. MYRG-GRG2024-00032-FST-UMDF) from the University of Macau.

References

Bain, A., Chan, M. N., and Bzdek, B. R.: Physical properties of short chain aqueous organosulfate aerosol, Environ. Sci. Atmos., 3, 1365-1373, https://doi.org/10.1039/d3ea00088e, 2023.

Barbosa, T. S., Riva, M., Chen, Y. Z., da Silva, C. M., Ameida, J. C. S., Zhang, Z., Gold, A., Arbilla, G., Bauerfeldt, G. F., and Surratt, J. D.: Chemical characterization of organosulfates from the hydroxyl radical-initiated oxidation and ozonolysis of cis-3-hexen-1-ol, Atmos. Environ., 162, 141-151, https://doi.org/10.1016/j.atmosenv.2017.04.026, 2017.

Bennett, J. E. and Summers, R.: Product studies of the mutual termination reactions of sec-alkylperoxy radicals: Evidence for non-cyclic termination, Can. J. Chem., 52, 1377-1379, https://doi.org/10.1139/v74-209, 1974.

Berruti, I., Polo-Lopez, M. I., Oller, I., Flores, J., Marin, M. L., and Bosca, F.: Sulfate radical anion: Laser flash photolysis study and application in water disinfection and decontamination, Appl. Catal. B-Environ., 315, 121519, https://doi.org/10.1016/j.apcatb.2022.121519, 2022.

Brüggemann, M., Van Pinxteren, D., Wang, Y., Yu, J. Z., and Herrmann, H.: Quantification of known and unknown terpenoid organosulfates in PM_{10} using untargeted LC–HRMS/MS: contrasting summertime rural Germany and the North China Plain, Environ. Chem., 16, 333-346, https://doi.org/10.1071/en19089, 2019.

Brüggemann, M., Xu, R., Tilgner, A., Kwong, K. C., Mutzel, A., Poon, H. Y., Otto, T., Schaefer, T., Poulain, L., Chan, M. N., and Herrmann, H.: Organosulfates in Ambient Aerosol: State of Knowledge and Future Research Directions on Formation, Abundance, Fate, and Importance, Environ. Sci. Technol., 54, 3767-3782, https://doi.org/10.1021/acs.est.9b06751, 2020.

Chen, Y. Z., Dombek, T., Hand, J., Zhang, Z. F., Gold, A., Ault, A. P., Levine, K. E., and Surratt, J. D.: Seasonal Contribution of Isoprene-Derived Organosulfates to Total Water-Soluble Fine Particulate Organic Sulfur in the United States, ACS Earth Space Chem., 5, 2419-2432, https://doi.org/10.1021/acsearthspacechem.1c00102, 2021.

Chen, Y. Z., Zhang, Y., Lambe, A. T., Xu, R. S., Lei, Z. Y., Olson, N. E., Zhang, Z. F., Szalkowski, T., Cui, T. Q., Vizuete, W., Gold, A., Turpin, B. J., Ault, A. P., Chan, M. N., and Surratt, J. D.: Heterogeneous Hydroxyl Radical Oxidation of Isoprene-Epoxydiol-Derived Methyltetrol Sulfates: Plausible Formation Mechanisms of Previously Unexplained Organosulfates in Ambient Fine Aerosols, Environ. Sci. Technol. Lett., 7, 460-468, https://doi.org/10.1021/acs.estlett.0c00276, 2020.

Choudhary, V., Roson, M. L., Guo, X. Y., Gautam, T., Gupta, T., and Zhao, R.: Aqueous-phase photochemical oxidation of water-soluble brown carbon aerosols arising from solid biomass fuel burning, Environ. Sci. Atmos., 3, 816-829, https://doi.org/10.1039/d2ea00151a, 2023.

Darer, A. I., Cole-Filipiak, N. C., O'Connor, A. E., and Elrod, M. J.: Formation and stability of atmospherically relevant isoprene-derived organosulfates and organonitrates, Environ. Sci. Technol., 45, 1895-1902, https://doi.org/10.1021/es103797z, 2011.

Doussin, J. F. and Monod, A.: Structure-activity relationship for the estimation of OH-oxidation rate constants of carbonyl compounds in the aqueous phase, Atmos. Chem. Phys., 13, 11625-11641, https://doi.org/10.5194/acp-13-11625-2013, 2013.

Fan, W., Chen, T., Zhu, Z., Zhang, H., Qiu, Y., and Yin, D.: A review of secondary organic aerosols formation focusing on organosulfates and organic nitrates, J. Hazard. Mater., 430, 128406, https://doi.org/10.1016/j.jhazmat.2022.128406, 2022.

George, I. J. and Abbatt, J. P.: Heterogeneous oxidation of atmospheric aerosol particles by gas-phase radicals, Nat. Chem., 2, 713-722, https://doi.org/10.1038/nchem.806, 2010.

Gweme, D. T. and Styler, S. A.: OH Radical Oxidation of Organosulfates in the Atmospheric Aqueous Phase, J. Phys. Chem. A., 128, 9462-9475, https://doi.org/10.1021/acs.jpca.4c02877, 2024.

Hansen, A. M. K., Hong, J., Raatikainen, T., Kristensen, K., Ylisirniö, A., Virtanen, A., Petäjä, T., Glasius, M., and Prisle, N. L.: Hygroscopic properties and cloud condensation nuclei activation of limonene-derived organosulfates and their mixtures with ammonium sulfate, Atmos. Chem. Phys., 15, 14071-14089, https://doi.org/10.5194/acp-15-14071-2015, 2015.

Hearn, J. D., Renbaum, L. H., Wang, X., and Smith, G. D.: Kinetics and products from reaction of Cl radicals with dioctyl sebacate (DOS) particles in O_2: a model for radical-initiated oxidation of organic aerosols, Phys. Chem. Chem. Phys., 9, 4803-4813, https://doi.org/10.1039/b707523e, 2007.

Hems, R. F. and Abbatt, J. P. D.: Aqueous Phase Photo-oxidation of Brown Carbon Nitrophenols: Reaction Kinetics, Mechanism, and Evolution of Light Absorption, ACS Earth Space Chem., 2, 225-234, https://doi.org/10.1021/acsearthspacechem.7b00123, 2018.

Herrmann, H., Hoffmann, D., Schaefer, T., Brauer, P., and Tilgner, A.: Tropospheric aqueous-phase free-radical chemistry: radical sources, spectra, reaction kinetics and prediction tools, ChemPhysChem., 11, 3796-3822, https://doi.org/10.1002/cphc.201000533, 2010.

Hettiyadura, A. P. S., Al-Naiema, I. M., Hughes, D. D., Fang, T., and Stone, E. A.: Organosulfates in Atlanta, Georgia: anthropogenic influences on biogenic secondary organic

aerosol formation, Atmos. Chem. Phys., 19, 3191-3206, https://doi.org/10.5194/acp-19-3191-2019, 2019.

Hu, K. S., Darer, A. I., and Elrod, M. J.: Thermodynamics and kinetics of the hydrolysis of atmospherically relevant organonitrates and organosulfates, Atmos. Chem. Phys., 11, 8307-8320, https://doi.org/10.5194/acp-11-8307-2011, 2011.

Huang, R. J., Cao, J. J., Chen, Y., Yang, L., Shen, J. C., You, Q. H., Wang, K., Lin, C. S., Xu, W., Gao, B., Li, Y. J., Chen, Q., Hoffmann, T., O'Dowd, C. D., Bilde, M., and Glasius, M.: Organosulfates in atmospheric aerosol: synthesis and quantitative analysis of PM from Xi'an, northwestern China, Atmos. Meas. Tech., 11, 3447-3456, https://doi.org/10.5194/amt-11-3447-2018, 2018.

Hughes, D. D., Christiansen, M. B., Milani, A., Vermeuel, M. P., Novak, G. A., Alwe, H. D., Dickens, A. F., Pierce, R. B., Millet, D. B., Bertram, T. H., Stanier, C. O., and Stone, E. A.: $PM_{2.5}$ chemistry, organosulfates, and secondary organic aerosol during the 2017 Lake Michigan Ozone Study, Atmos. Environ., 244, 117939, https://doi.org/10.1016/j.atmosenv.2020.117939, 2021.

Iinuma, Y., Müller, C., Böge, O., Gnauk, T., and Herrmann, H.: The formation of organic sulfate esters in the limonene ozonolysis secondary organic aerosol (SOA) under acidic conditions, Atmos. Environ., 41, 5571-5583, https://doi.org/10.1016/j.atmosenv.2007.03.007, 2007.

Jiang, H. X., Li, J., Tang, J., Cui, M., Zhao, S. Z., Mo, Y. Z., Tian, C. G., Zhang, X. Y., Jiang, B., Liao, Y. H., Chen, Y. J., and Zhang, G.: Molecular characteristics, sources, and formation pathways of organosulfur compounds in ambient aerosol in Guangzhou, South China, Atmos. Chem. Phys., 22, 6919-6935, https://doi.org/10.5194/acp-22-6919-2022, 2022.

Jiang, W. Q., Niedek, C., Anastasio, C., and Zhang, Q.: Photoaging of phenolic secondary organic aerosol in the aqueous phase:evolution of chemical and optical properties and effects of oxidants, Atmos. Chem. Phys., 23, 7103-7120, https://doi.org/10.5194/acp-23-7103-2023, 2023.

Kessler, S. H., Nah, T., Daumit, K. E., Smith, J. D., Leone, S. R., Kolb, C. E., Worsnop, D. R., Wilson, K. R., and Kroll, J. H.: OH-initiated heterogeneous aging of highly oxidized organic aerosol, J. Phys. Chem. A., 116, 6358-6365, https://doi.org/10.1021/jp212131m, 2012.

Kristensen, K. and Glasius, M.: Organosulfates and oxidation products from biogenic hydrocarbons in fine aerosols from a forest in North West Europe during spring, Atmos. Environ., 45, 4546-4556, https://doi.org/10.1016/j.atmosenv.2011.05.063, 2011.

Kroll, J. H., Lim, C. Y., Kessler, S. H., and Wilson, K. R.: Heterogeneous Oxidation of Atmospheric Organic Aerosol: Kinetics of Changes to the Amount and Oxidation State of Particle-Phase Organic Carbon, J. Phys. Chem. A., 119, 10767-10783, https://doi.org/10.1021/acs.jpca.5b06946, 2015.

5   Kroll, J. H., Smith, J. D., Che, D. L., Kessler, S. H., Worsnop, D. R., and Wilson, K. R.: Measurement of fragmentation and functionalization pathways in the heterogeneous oxidation of oxidized organic aerosol, Phys. Chem. Chem. Phys., 11, 8005-8014, https://doi.org/10.1039/b905289e, 2009.

Kroll, J. H., Donahue, N. M., Jimenez, J. L., Kessler, S. H., Canagaratna, M. R., Wilson, K. R.,
10   Altieri, K. E., Mazzoleni, L. R., Wozniak, A. S., Bluhm, H., Mysak, E. R., Smith, J. D., Kolb, C. E., and Worsnop, D. R.: Carbon oxidation state as a metric for describing the chemistry of atmospheric organic aerosol, Nat. Chem., 3, 133-139, https://doi.org/10.1038/nchem.948, 2011.

Kwong, K. C., Chim, M. M., Davies, J. F., Wilson, K. R., and Chan, M. N.: Importance of sulfate radical anion formation and chemistry in heterogeneous OH oxidation of sodium methyl
15   sulfate, the smallest organosulfate, Atmos. Chem. Phys., 18, 2809-2820, https://doi.org/10.5194/acp-18-2809-2018, 2018.

Lai, D. E., Schaefer, T., Zhang, Y. M., Li, Y. J., Herrmann, H., and Chan, M. N.: Oxidation Kinetics of Alkyl Sulfates and Sulfonates by Sulfate Radical ($SO_4^{\bullet-}$) in the Aqueous Phase: Deactivating Role of Sulfur Functional Groups, ACS Earth Space Chem., 9, 158-168,
20   https://doi.org/10.1021/acsearthspacechem.4c00313, 2025.

Lai, D. E., Schaefer, T., Zhang, Y. M., Li, Y. J., Xing, S. N., Herrmann, H., and Chan, M. N.: Deactivating Effect of Hydroxyl Radicals Reactivity by Sulfate and Sulfite Functional Groups in Aqueous Phase ─ Atmospheric Implications for Small Organosulfur Compounds, ACS ES&T Air., 1, 7, 678–689, https://doi.org/10.1021/acsestair.4c00033, 2024.

25   Lai, D. E., Wong, Y. K., Xu, R. S., Xing, S. N., Ng, S. I. M., Kong, L., Yu, J. Z., Huang, D. D., and Chan, M. N.: Significant Conversion of Organic Sulfur from Hydroxymethanesulfonate to Inorganic Sulfate and Peroxydisulfate Ions upon Heterogeneous OH Oxidation, Environ. Sci. Technol. Lett., 10, 773-778, https://doi.org/10.1021/acs.estlett.3c00472, 2023.

Lambe, A. T., Onasch, T. B., Croasdale, D. R., Wright, J. P., Martin, A. T., Franklin, J. P.,
30   Massoli, P., Kroll, J. H., Canagaratna, M. R., Brune, W. H., Worsnop, D. R., and Davidovits, P.: Transitions from functionalization to fragmentation reactions of laboratory secondary organic aerosol (SOA) generated from the OH oxidation of alkane precursors, Environ. Sci. Technol., 46, 5430-5437, https://doi.org/10.1021/es300274t, 2012.

Ma, Y., Xu, X. K., Song, W. H., Geng, F. H., and Wang, L.: Seasonal and diurnal variations of particulate organosulfates in urban Shanghai, China, Atmos. Environ., 85, 152-160, https://doi.org/10.1016/j.atmosenv.2013.12.017, 2014.

Mackay, D. and Shiu, W. Y.: A critical review of Henry's law constants for chemicals of environmental interest, J. Phys. Chem. Ref. Data., 10, 1175-1199, https://doi.org/10.1063/1.555654, 1981.

Minerath, E. C., Casale, M. T., and Elrod, M. J.: Kinetics feasibility study of alcohol sulfate esterification reactions in tropospheric aerosols, Environ. Sci. Technol., 42, 4410-4415, https://doi.org/10.1021/es8004333, 2008.

Monod, A. and Doussin, J. F.: Structure-activity relationship for the estimation of OH-oxidation rate constants of aliphatic organic compounds in the aqueous phase: alkanes, alcohols, organic acids and bases, Atmos. Environ., 42, 7611-7622, https://doi.org/10.1016/j.atmosenv.2008.06.005, 2008.

Ng, S. I. M. and Chan, M. N.: Beyond the formation: unveiling the atmospheric transformation of organosulfates via heterogeneous OH oxidation, Chem. Commun., 59, 13919-13938, https://doi.org/10.1039/D3CC03700B, 2023.

Ng, S. I. M., Ng, K. H., Yeung, P. W. F., Xu, R. S., So, P. K., Huang, Y. L., Yu, J. Z., Choi, C. K. K., Tse, Y. L. S., and Chan, M. N.: Chemical transformation of a long-chain alkyl organosulfate heterogeneous OH oxidation: a case study of sodium dodecyl sulfate, Environ. Sci. Atmos., 2, 1060-1075, https://doi.org/10.1039/d2ea00026a, 2022.

Nozière, B., Ekström, S., Alsberg, T., and Holmström, S.: Radical-initiated formation of organosulfates and surfactants in atmospheric aerosols, Geophys. Res. Lett., 37, https://doi.org/10.1029/2009GL041683, 2010.

Otto, T., Schaefer, T., and Herrmann, H.: Aqueous-Phase Oxidation of cis-beta-Isoprene Epoxydiol by Hydroxyl Radicals and Its Impact on Atmospheric Isoprene Processing, J. Phys. Chem. A., 123, 10599-10608, https://doi.org/10.1021/acs.jpca.9b08836, 2019.

Passananti, M., Kong, L., Shang, J., Dupart, Y., Perrier, S., Chen, J., Donaldson, D. J., and George, C.: Organosulfate Formation through the Heterogeneous Reaction of Sulfur Dioxide with Unsaturated Fatty Acids and Long-Chain Alkenes, Angew. Chem. Int. Edit., 55, 10336-10339, https://doi.org/10.1002/anie.201605266, 2016.

Perri, M. J., Lim, Y. B., Seitzinger, S. P., and Turpin, B. J.: Organosulfates from glycolaldehyde in aqueous aerosols and clouds: Laboratory studies, Atmos. Environ., 44, 2658-2664, https://doi.org/10.1016/j.atmosenv.2010.03.031, 2010.

Riva, M., Barbosa, T. D., Lin, Y. H., Stone, E. A., Gold, A., and Surratt, J. D.: Chemical characterization of organosulfates in secondary organic aerosol derived from the photooxidation of alkanes, Atmos. Chem. Phys., 16, 11001-11018, https://doi.org/10.5194/acp-16-11001-2016, 2016.

5   Riva, M., Chen, Y., Zhang, Y., Lei, Z., Olson, N. E., Boyer, H. C., Narayan, S., Yee, L. D., Green, H. S., and Cui, T.: Increasing isoprene epoxydiol-to-inorganic sulfate aerosol ratio results in extensive conversion of inorganic sulfate to organosulfur forms: implications for aerosol physicochemical properties, Environ. Sci. Technol., 53, 8682-8694, https://doi.org/10.1021/acs.est.9b01019, 2019.

10   Russell, G. A.: Deuterium-isotope effects in the autoxidation of aralkyl hydrocarbons. mechanism of the interaction of peroxy radicals[1], J. Am. Chem. Soc., 79, 3871-3877, https://doi.org/10.1021/ja01571a068, 1957.

Schindelka, J., Iinuma, Y., Hoffmann, D., and Herrmann, H.: Sulfate radical-initiated formation of isoprene-derived organosulfates in atmospheric aerosols, Faraday. Discuss., 165,

15   237-259, https://doi.org/10.1039/c3fd00042g, 2013.

Shang, J., Passananti, M., Dupart, Y., Ciuraru, R., Tinel, L., Rossignol, S., Perrie, S., Zhu, T., and George, C.: SO$_2$ Uptake on Oleic Acid: A New Formation Pathway of Organosulfur Compounds in the Atmosphere, Environ. Sci. Technol. Lett., 3, 67-72, https://doi.org/10.1021/acs.estlett.6b00006, 2016.

20   Shrivastava, M., Cappa, C. D., Fan, J. W., Goldstein, A. H., Guenther, A. B., Jimenez, J. L., Kuang, C., Laskin, A., Martin, S. T., Ng, N. L., Petaja, T., Pierce, J. R., Rasch, P. J., Roldin, P., Seinfeld, J. H., Shilling, J., Smith, J. N., Thornton, J. A., Volkamer, R., Wang, J., Worsnop, D. R., Zaveri, R. A., Zelenyuk, A., and Zhang, Q.: Recent advances in understanding secondary organic aerosol: Implications for global climate forcing, Rev. Geophys., 55, 509-559,

25   https://doi.org/10.1002/2016rg000540, 2017.

Smith, J., Kroll, J., Cappa, C., Che, D., Liu, C., Ahmed, M., Leone, S., Worsnop, D., and Wilson, K.: The heterogeneous reaction of hydroxyl radicals with sub-micron squalane particles: a model system for understanding the oxidative aging of ambient aerosols, Atmos. Chem. Phys., 9, 3209-3222, https://doi.org/10.5194/acp-9-3209-2009, 2009.

30   Surratt, J. D., Chan, A. W., Eddingsaas, N. C., Chan, M., Loza, C. L., Kwan, A. J., Hersey, S. P., Flagan, R. C., Wennberg, P. O., and Seinfeld, J. H.: Reactive intermediates revealed in secondary organic aerosol formation from isoprene, Proc. Natl. Acad. Sci. U.S.A., 107, 6640-6645, https://doi.org/10.1073/pnas.0911114107, 2010.

Surratt, J. D., Kroll, J. H., Kleindienst, T. E., Edney, E. O., Claeys, M., Sorooshian, A., Ng, N. L., Offenberg, J. H., Lewandowski, M., Jaoui, M., Flagan, R. C., and Seinfeld, J. H.: Evidence for organosulfates in secondary organic aerosol, Environ. Sci. Technol., 41, 517-527, https://doi.org/10.1021/es062081q, 2007.

5 Surratt, J. D., Gomez-Gonzalez, Y., Chan, A. W., Vermeylen, R., Shahgholi, M., Kleindienst, T. E., Edney, E. O., Offenberg, J. H., Lewandowski, M., Jaoui, M., Maenhaut, W., Claeys, M., Flagan, R. C., and Seinfeld, J. H.: Organosulfate formation in biogenic secondary organic aerosol, J. Phys. Chem. A., 112, 8345-8378, https://doi.org/10.1021/jp802310p, 2008.

Szmigielski, R.: Evidence for C_5 organosulfur secondary organic aerosol components from in-
10 cloud processing of isoprene: Role of reactive SO_4 and SO_3 radicals, Atmos. Environ., 130, 14-22, https://doi.org/10.1016/j.atmosenv.2015.10.072, 2016.

Wach, P., Spolnik, G., Rudzinski, K. J., Skotak, K., Claeys, M., Danikiewicz, W., and Szmigielski, R.: Radical oxidation of methyl vinyl ketone and methacrolein in aqueous droplets: Characterization of organosulfates and atmospheric implications, Chemosphere, 214, 1-9,
15 https://doi.org/10.1016/j.chemosphere.2018.09.026, 2019.

Wang, Y., Ren, J., Huang, X. H. H., Tong, R., and Yu, J. Z.: Synthesis of Four Monoterpene-Derived Organosulfates and Their Quantification in Atmospheric Aerosol Samples, Environ. Sci. Technol., 51, 6791-6801, https://doi.org/10.1021/acs.est.7b01179, 2017.

Wang, Y., Ma, Y., Kuang, B., Lin, P., Liang, Y., Huang, C., and Yu, J. Z.: Abundance of
20 organosulfates derived from biogenic volatile organic compounds: Seasonal and spatial contrasts at four sites in China, Sci. Total. Environ., 806, 151275, https://doi.org/10.1016/j.scitotenv.2021.151275, 2022.

Wang, Y., Ma, Y., Li, X., Kuang, B. Y., Huang, C., Tong, R., and Yu, J. Z.: Monoterpene and sesquiterpene α-hydroxy organosulfates: synthesis, MS/MS characteristics, and ambient
25 presence, Environ. Sci. Technol., 53, 12278-12290, https://doi.org/10.1021/acs.est.9b04703, 2019.

Wang, Y., Hu, M., Guo, S., Wang, Y., Zheng, J., Yang, Y., Zhu, W., Tang, R., Li, X., and Liu, Y.: The secondary formation of organosulfates under interactions between biogenic emissions and anthropogenic pollutants in summer in Beijing, Atmos. Chem. Phys., 18, 10693-10713,
30 https://doi.org/10.5194/acp-18-10693-2018, 2018.

Wen, L., Schaefer, T., He, L., Zhang, Y. M., Sun, X. M., Ventura, O. N., and Herrmann, H.: T- and pH-Dependent Kinetics of the Reactions of $^\bullet OH_{(aq)}$ with Glutaric and Adipic Acid for Atmospheric Aqueous-Phase Chemistry, ACS Earth Space Chem., 5, 1854-1864, https://doi.org/10.1021/acsearthspacechem.1c00163, 2021.

Wiegel, A. A., Wilson, K. R., Hinsberg, W. D., and Houle, F. A.: Stochastic methods for aerosol chemistry: a compact molecular description of functionalization and fragmentation in the heterogeneous oxidation of squalane aerosol by OH radicals, Phys. Chem. Chem. Phys., 17, 4398-4411, https://doi.org/10.1039/c4cp04927f, 2015.

5   Wilson, K. R., Smith, J. D., Kessler, S. H., and Kroll, J. H.: The statistical evolution of multiple generations of oxidation products in the photochemical aging of chemically reduced organic aerosol, Phys. Chem. Chem. Phys., 14, 1468-1479, https://doi.org/10.1039/c1cp22716e, 2012.

Witkowski, B. and Gierczak, T.: cis-Pinonic Acid Oxidation by Hydroxyl Radicals in the Aqueous Phase under Acidic and Basic Conditions: Kinetics and Mechanism, Environ. Sci.

10   Technol., 51, 9765-9773, https://doi.org/10.1021/acs.est.7b02427, 2017.

Witkowski, B., Jurdana, S., and Gierczak, T.: Limononic Acid Oxidation by Hydroxyl Radicals and Ozone in the Aqueous Phase, Environ. Sci. Technol., 52, 3402-3411, https://doi.org/10.1021/acs.est.7b04867, 2018.

Witkowski, B., Al-Sharafi, M., Błaziak, K., and Gierczak, T.: Aging of α-Pinene Secondary

15   Organic Aerosol by Hydroxyl Radicals in the Aqueous Phase: Kinetics and Products, Environ. Sci. Technol., 57, 6040-6051, https://doi.org/10.1021/acs.est.2c07630, 2023.

Witkowski, B., Jain, P., Wileńska, B., and Gierczak, T.: Temperature-dependent aqueous OH kinetics of C2–C10 linear and terpenoid alcohols and diols: new rate coefficients, structure–activity relationship, and atmospheric lifetimes, Atmos. Chem. Phys., 24, 663-688,

20   https://doi.org/10.5194/acp-24-663-2024, 2024.

Xu, R. S., Chen, Y., Ng, S. I. M., Zhang, Z., Gold, A., Turpin, B. J., Ault, A. P., Surratt, J. D., and Chan, M. N.: Formation of Inorganic Sulfate and Volatile Nonsulfated Products from Heterogeneous Hydroxyl Radical Oxidation of 2-Methyltetrol Sulfate Aerosols: Mechanisms and Atmospheric Implications, Environ. Sci. Technol. Lett., 11, 968-974,

25   https://doi.org/10.1021/acs.estlett.4c00451, 2024.

Xu, R. S., Ng, S. I. M., Chow, W. S., Wong, Y. K., Wang, Y. C., Lai, D., Yao, Z. P., So, P. K., Yu, J. Z., and Chan, M. N.: Chemical transformation of α-pinene-derived organosulfate via heterogeneous OH oxidation: implications for sources and environmental fates of atmospheric organosulfates, Atmos. Chem. Phys., 22, 5685-5700, https://doi.org/10.5194/acp-22-5685-

30   2022, 2022.

Yang, T., Xu, Y., Ma, Y. J., Wang, Y. C., Yu, J. Z., Sun, Q. B., Xiao, H. W., Xiao, H. Y., and Liu, C. Q.: Field Evidence for Constraints of Nearly Dry and Weakly Acidic Aerosol Conditions on the Formation of Organosulfates, Environ. Sci. Technol. Lett., 11, 981-987, https://doi.org/10.1021/acs.estlett.4c00522, 2024.

Yttri, K. E., Simpson, D., Nojgaard, J. K., Kristensen, K., Genberg, J., Stenström, K., Swietlicki, E., Hillamo, R., Aurela, M., Bauer, H., Offenberg, J. H., Jaoui, M., Dye, C., Eckhardt, S., Burkhart, J. F., Stohl, A., and Glasius, M.: Source apportionment of the summer time carbonaceous aerosol at Nordic rural background sites, Atmos. Chem. Phys., 11, 13339-13357, https://doi.org/10.5194/acp-11-13339-2011, 2011.

Zhang, H., Worton, D. R., Lewandowski, M., Ortega, J., Rubitschun, C. L., Park, J. H., Kristensen, K., Campuzano-Jost, P., Day, D. A., Jimenez, J. L., Jaoui, M., Offenberg, J. H., Kleindienst, T. E., Gilman, J., Kuster, W. C., de Gouw, J., Park, C., Schade, G. W., Frossard, A. A., Russell, L., Kaser, L., Jud, W., Hansel, A., Cappellin, L., Karl, T., Glasius, M., Guenther, A., Goldstein, A. H., Seinfeld, J. H., Gold, A., Kamens, R. M., and Surratt, J. D.: Organosulfates as tracers for secondary organic aerosol (SOA) formation from 2-methyl-3-buten-2-ol (MBO) in the atmosphere, Environ. Sci. Technol., 46, 9437-9446, https://doi.org/10.1021/es301648z, 2012.

Zhu, M., Jiang, B., Li, S., Yu, Q. Q., Yu, X., Zhang, Y. L., Bi, X. H., Yu, J. Z., George, C., Yu, Z. Q., and Wang, X. M.: Organosulfur Compounds Formed from Heterogeneous Reaction between SO_2 and Particulate-Bound Unsaturated Fatty Acids in Ambient Air, Environ. Sci. Technol. Lett., 6, 318-322, https://doi.org/10.1021/acs.estlett.9b00218, 2019.